Insights into specificity of cleavage and mechanism of cell entry from the crystal structure of the highly specific *Aspergillus* ribotoxin, restrictocin

Xiaojing Yang† and Keith Moffat*

Background: Restrictocin, a highly specific ribotoxin made by the fungus *Aspergillus restrictus,* cleaves a single phosphodiester bond in the 28S RNA of eukaryotic ribosomes, inhibiting protein synthesis. The sequence around this cleavage site is a binding site for elongation factors, and is conserved in all cytoplasmic ribosomes. The catalytic mechanism of restrictocin and the reasons for its high substrate specificity are unknown. No structure has been determined for any other member of the *Aspergillus* ribotoxin family.

Results: The crystal structure of restrictocin was determined at 2.1 Å resolution by single isomorphous replacement and anomalous scattering techniques, and refined to 1.7 Å resolution using synchrotron Laue data. The structural core of the protein, in which a three-turn α helix is packed against a five-stranded antiparallel β sheet, can be well aligned with that of ribonuclease T1. Large positively charged peripheral loops near the active site construct a platform with a concave surface for RNA binding.

Conclusions: Restrictocin appears to combine the catalytic components of T1 ribonucleases with the base recognition components of Sa ribonucleases. Modeling studies using an NMR structure of an RNA substrate analog suggest that the tertiary structure of the substrate RNA is important in protein–RNA recognition, fitting closely into the concavity of the presumed binding site. We speculate that the large 39-residue loop L3, which has similarities to loops found in lectin sugar-binding domains, may be responsible for restrictocin's ability to cross cell membranes.

Address: Department of Biochemistry and Molecular Biology, The University of Chicago, 920 East 58th Street, Chicago, Illinois 60637, USA.

†Present address: Department of Biochemistry, Molecular Biology and Cell Biology, Northwestern University, 2153 Sheridan Road, Evanston, Illinois 60208, USA.

*Corresponding author.
E-mail: moffat@cars.uchicago.edu

Key words: cell-entry activity, Laue diffraction, protein–RNA specific recognition, ribotoxins, SIRAS

Received: 12 April 1996
Revisions requested: 25 April 1996
Revisions received: 31 May 1996
Accepted: 31 May 1996

Structure 15 July 1996, 4:837–852

 ISSN 0969-2126

Introduction

Restrictocin is a basic cytotoxic protein of 149 amino acids produced by the fungus *Aspergillus restrictus*. It belongs to a specific class of ribosome-inactivating proteins (RIPs) that can specifically cleave a single phosphodiester bond in 28S rRNA of the eukaryotic large ribosomal subunit and inhibit protein synthesis [1]. Other members of this class of proteins are mitogillin from another strain of *A. restrictus*, α-sarcin from *Aspergillus giganteus* and *aspf1* from *Aspergillus fumigatus* [2,3]. They are often referred to as the '*Aspergillus* ribotoxins'. Restrictocin differs in only one residue from mitogillin and shares 86% sequence identity with α-sarcin [4].

The restrictocin cleavage site in 28S rRNA is located on the 3′ side of a guanosine residue in the sequence AGUACGAG|AGGAAG [5]. This 14-nucleotide purine-rich sequence, called the 'α-sarcin domain', is universally conserved in cytoplasmic large subunit rRNAs [5]. The α-sarcin domain is suggested to be a very important site in protein synthesis. This domain is a major target for many other ribotoxins, such as ricin, abrin, modeccin and trichosanthin (from higher plants), shiga toxin (from *Shigella dysenteriae*), verotoxins 1 and 2 (from *Escherichia coli*) and tricholin (from *Trichoderma viride*). Despite their quite different enzymatic activities these toxins all target the same domain [6-8]. Direct evidence for the further importance of this domain comes from footprinting experiments, in which elongation factors EF-1 and EF-2 (EF-Tu and EF-G in prokaryotes) were found to bind the same α-sarcin domain of ribosomes [9,10]. Inhibition of protein synthesis by the *Aspergillus* ribotoxins involves both prevention of EF-1-dependent binding of aminoacyl tRNA and GTP-dependent binding of EF-2 to their ribosomal sites [11,12].

The most distinctive feature of the *Aspergillus* ribotoxins as ribonucleases is their exceptionally high specificity for a single phosphodiester bond within eukaryotic large subunit rRNAs. Endo and Wool [13] showed that the cleavage site of α-sarcin is located 393 nucleotides from the 3′ end of the 28S rRNA and generates 3′ phosphate and 5′ hydroxyl products. Compared to other ribonucleases, restrictocin shares 24% sequence identity with RNase T1 (T1) and 34% with RNase U2 (U2) [14]. Many of the conserved residues are concentrated near the catalytic site of T1 and U2, suggesting that a similar enzymatic mechanism holds for the *Aspergillus* ribotoxins.

Extensive studies on substrate specificity have been carried out using a synthetic oligoribonucleotide (35-mer) that reproduces the conserved nucleotides, and presumably the secondary structure, of the α-sarcin domain of ribosomes [15]. To retain substrate specificity, a stem containing a minimum of three base pairs [16] and a guanine base, six bases 5′ to the cleavage site, were found to be essential [17]. In contrast, the bases around the cleavage site can be altered without greatly affecting the substrate specificity. These results strongly suggest that the tertiary structure of the α-sarcin domain stem and loop, rather than a simple conserved sequence, plays a critical role in specific protein–RNA recognition.

How the *Aspergillus* ribotoxins get into cells to exhibit their toxicity is not yet known. Toxins, like diphtheria toxin, enterotoxin and ricin, either have distinctive domains for receptor binding and translocation or employ a second polypeptide chain to facilitate the translocation of the catalytic subunit across the cell membrane [18-20]. In contrast, restrictocin, mitogillin and α-sarcin are small basic proteins consisting of a single polypeptide chain. α-Sarcin has substantially limited activity against intact cells, although it is an effective inhibitor of *in vivo* protein synthesis: in virus-infected cells [21,22]; in many tumor cell lines [23], and in cells whose membrane permeability has been modified by treatment with phospholipase C or external ATP [24]. No cell surface receptors have so far been identified which might be involved in the translocation of the ribotoxins. Studies on α-sarcin, using model membrane systems, suggest that interactions between α-sarcin and acidic phospholipids in membranes play an important role in the cell-entry activity of the *Aspergillus* ribotoxins [23,25-27].

It has recently been suggested that restrictocin is an insect antagonist as it protects *A. restrictus* conidiophores from insects that feed on fungi [28]. Restrictocin has also been implicated in the pathogenesis of human aspergillosis, a condition caused by *A. fumigatus* [29]. *Aspf1*, a protein differing in only two amino acid residues from restrictocin, was shown to be the major antigen in the urine of patients with invasive pulmonary aspergillosis. The expression of both *aspf1* protein and its mRNA in *A. fumigatus* and *A. restrictus* (but not in other species of *Aspergillus*) [30] suggested that *aspf1* is a potential virulence factor for *A. fumigatus*-related diseases. These diseases account for 80% of cases of human aspergillosis.

We have determined the crystal structure of restrictocin at 2.1 Å resolution by single isomorphous replacement and anomalous scattering techniques (SIRAS). The structure was refined to 1.7 Å resolution using synchrotron Laue data. This restrictocin structure is the first crystal structure determined for a member of the *Aspergillus* ribotoxin family. With this crystal structure, we aim to understand the catalytic mechanism, substrate specificity and cell-entry activity of restrictocin.

Results

Quality of the model

Two restrictocin molecules in the asymmetric unit were independently built from the solvent-flattened, figure of merit weighted Fo map, calculated from SIRAS phases at 2.1 Å resolution. This map was readily interpreted, Figure 1a shows a typical region of the experimental solvent-flattened SIRAS map. The model was refined using cycles of iterative manual rebuilding and automatic refinement with X-PLOR protocols [31] against both the monochromatic FAST data at 2.1 Å resolution and the synchrotron Laue data at 1.7 Å resolution. For the two molecules in one asymmetric unit, the final model consists of 285 amino acid residues, three phosphate groups and 204 water molecules. The crystallographic R factor is 17.7% using synchrotron Laue data with $F/\sigma F >= 2$ in the 8.0–1.7 Å resolution range with a free R factor of 23.7%. Figure 1b shows the same region as in Figure 1a in the final 2Fo–Fc map calculated with the refined phases at 1.7 Å resolution using synchrotron Laue data. This map is of excellent quality; holes can be seen in many aromatic side chains and even in some proline residues at the 1σ contour level. Most water molecules are ordered and can be found in both molecules of restrictocin. The electron density for all carbonyl oxygen atoms is very well defined so that *cis*-prolines (Pro48, Pro112 and Pro126) can be easily assigned. The real space correlation coefficients for most residues are greater than 0.95, indicating a very good fit between the model and the 2Fo–Fc map. No residues, other than glycines and prolines, are found beyond the allowed regions in a Ramachandran plot. The average error of the atomic coordinates is about 0.18 Å as estimated by a Luzzati plot. The average temperature factors for the main-chain and side-chain atoms are 19.9 $Å^2$ and 20.8 $Å^2$, respectively. Six residues located within a loop region are not visible in either molecule in the asymmetric unit. This is presumably because these residues are highly exposed to solvent and adopt numerous spatially distinct conformations. The overall root mean square (rms) deviation between the main-chain atoms of two monomers in the asymmetric unit is 0.52 Å, indicating that they have almost identical main-chain conformations.

Overall features

Restrictocin is an α+β structure with approximate molecular dimensions 35×27×26 Å (Fig. 2a). A stereoview of the Cα trace of restrictocin is shown in Figure 2c. The structural core consists of a five-stranded antiparallel β sheet (strands B3, B4, B5, B6 and B7) stabilized by a three-turn α helix (H1) in a perpendicular position. The curved β strands are highly twisted in a right-handed manner and form a shallow cleft. The twist is stabilized by a cluster of hydrophobic residues (Phe51, Ile68, Phe70, Ile122, Val134, Leu144 and Leu146) that are tightly packed in

Figure 1

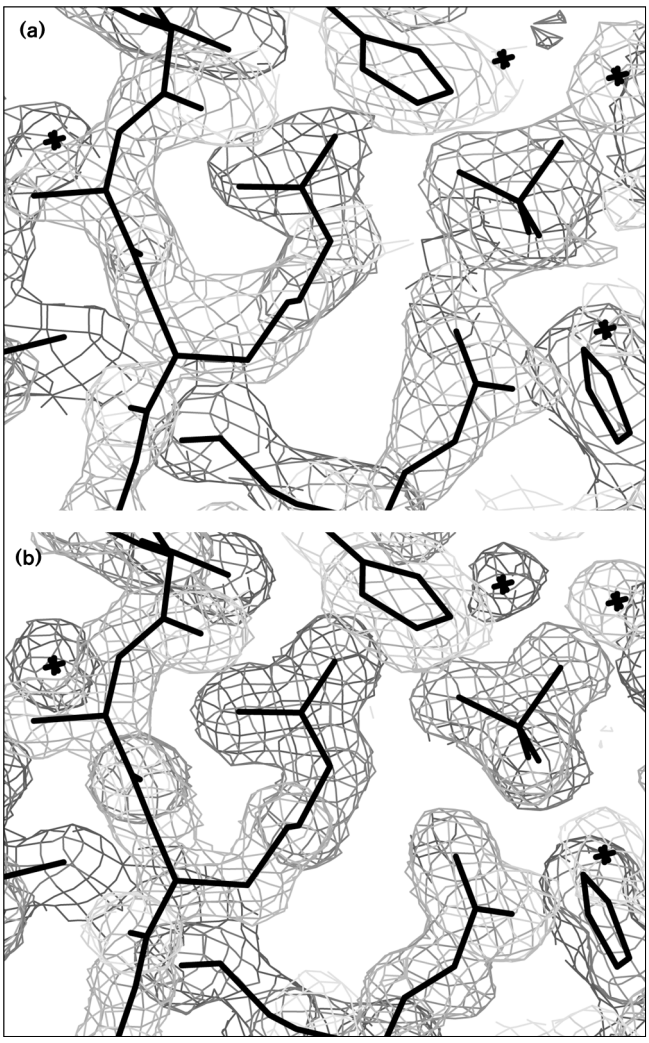

Quality of the electron-density maps. (a) One typical region of the experimental fom*Fo SIRAS map at 2.1 Å resolution. The map is contoured at 1σ level. The tetrahedron at the upper right of the figure represents a phosphate group and stars represent water molecules. (b) The same region in the 2Fo–Fc map at 1.7 Å resolution contoured at 1σ level. Both maps are displayed by *Xfit* in the program *XtalView* [61].

the narrow end of the cleft. At the open end of the cleft, the putative catalytic residues (His49, Glu95, Arg120 and His136) are found. These residues all point towards an inorganic phosphate group derived from the crystallization buffer (Fig. 2b).

Another long, two-stranded antiparallel β sheet (strands B1 and B2) is located at the N terminus of the structure and immediately before the three-turn helix (H1). The six residues which were not visible in the electron-density map are located in the turn of loop L1 between strands B1 and B2. Interestingly, the first two residues of helix H1, Ser25 and Gln26, also form part of strand B2; Ala1 O in strand B1 forms hydrogen bonds with Gln26 N and is involved in the N-capping of helix H1. In addition, the N-terminal strand B1 and the C-terminal strand B7 are linked by a disulfide bond (Cys5–Cys147), which stabilizes the termini. A very distinctive feature of restrictocin is the presence of large connecting loops between β strands. Loops L2 and L4 interact with each other at the entrance to the catalytic center (Fig. 2a). A 40-residue, glycine rich loop (L3) between strands B3 and B4 forms an independent structural domain. This domain is linked to the structural core by a disulfide bond (Cys75–Cys131) and by the hydrophobic residue cluster at the closed end of the cleft (Fig. 2b).

Structural alignments with other ribonucleases

As a ribonuclease, restrictocin was suggested to share a similar enzymatic mechanism with T1 and U2 [14]. While T1 and U2 specifically cleave at guanine bases, restrictocin only cleaves a single phosphodiester bond in 28S rRNA in the large ribosomal subunit and is specific for purines in naked RNAs [13]. The antiparallel β sheet and an adjacent long α helix which form the structural core of restrictocin also represent a common structure motif found in other ribonucleases including T1, RNase Ms (Ms), RNase Sa (Sa), and barnase [32]. In restrictocin the major β sheet and helix H1 are held together by a hydrophobic core formed by Ala29 and Ala36 (from helix H1) and Phe96, Phe107, Val121, Phe130 and Ile133 (from β strands). With a least squares procedure (LSQKAB in the CCP4 package) we have aligned the restrictocin structure against those of ribonucleases T1, Ms, F1, Sa and barnase [33–37]. The rms deviations between equivalent elements (limited by a 2.0 Å cut-off) are listed in Tables 1,2. Sixty-two residues are equivalent between restrictocin and T1, Ms and F1. The substantial structural overlaps are observed in the regions of both termini, helix H1, the major β sheet and in loops L2 and L5 (Fig. 3a). In addition, the disulfide bond that links the N and C termini is conserved. Despite these extensive similarities, structural differences between restrictocin and T1 are prominent. The N-terminal antiparallel β strands (B1 and B2) and the linking loop (L1) in restrictocin are, in total, 18 residues longer than the corresponding elements of T1. Helix H1 in restrictocin is one turn shorter than in T1 due to the presence of a proline residue at the C terminus of the helix sequence. However, the most striking differences between restrictocin and T1 are found in the peripheral loops. Loops L3 and L4 in restrictocin are significantly larger than those in T1 and, despite their similar size, loops L2 and L6 adopt different conformations from those in T1.

In contrast, only 18 residues can be reasonably well aligned between restrictocin and Sa, barnase and RNase St (Table 2). Most of the conserved residues are located in the major β sheet and very close to the catalytic center. Neither Sa or barnase has the N-terminal antiparallel β sheet. Instead, the N-terminal residues in Sa form an additional β strand within the major antiparallel β sheet. In barnase there are

Figure 2

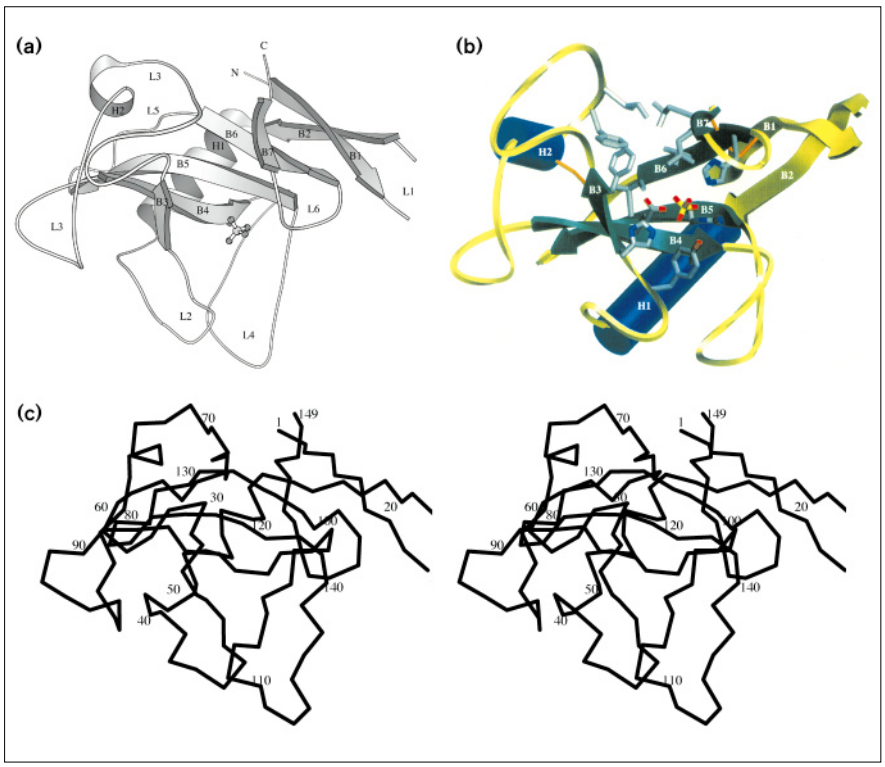

The structure of restrictocin. (a) Ribbon diagram of the restrictocin crystal structure (generated with the program MOLSCRIPT [66]). Assignment of the secondary structure elements and the residues they contain are as follows: B1: 1–10; L1: 11–16; B2: 17–24; H1: 25–35; L2: 36–48; B3: 49–52; L3: 53–91; H2: 73–77; B4: 92–98; L4: 99–117; B5: 118–125; L5: 126–131; B6: 132–137; L6: 138–142; B7: 143–147. (b) Ribbon diagram of restrictocin showing a view of the cleft. Helices are depicted in blue, the N-terminal β sheet is in yellow and the main β sheet of the core is in green. At the open end of the cleft, the catalytic residues are shown in gray with oxygen and nitrogen atoms in standard colors. These residues point to a phosphate group (the tetrahedron shown in yellow and red). The other end of the cleft is blocked by a cluster of hydrophobic residues (in gray). The disulfide bonds are in orange. (Figure produced with the program SETOR [67]). (c) Stereoview of a Cα trace of restrictocin, every tenth amino acid residue is numbered. The electron density corresponding to six residues in loop L1 could not be visualized in either molecule in the asymmetric unit and these residues are consequently missing in the atomic model. See the text.

three consecutive α helices at the N terminus, one of which is in a position comparable to helix H1 in restrictocin. The topologically comparable long helix in Sa is displaced from helix H1 in restrictocin by about 20° (Fig. 3b).

The active site

In the crystal structure of restrictocin, the putative catalytic residues, His49, Glu58, Arg120 and His136, come from different β strands in the major β sheet and line up across this sheet (Fig. 2b). The side chains of these residues cluster together at the open end of the cleft and point towards a tetrahedral-shaped electron density. This density was interpreted as an inorganic phosphate group derived from the crystallization buffer. His49 Nδ1 forms a hydrogen bond with the carbonyl oxygen of the next residue (Trp50 O); His49 Nε2 interacts with a phosphate oxygen (PO_4 O1). Trp47 OH is also hydrogen bonded to PO_4 O1, benefited by the conformation of *cis*-Pro48. Glu95 Oε2 is associated with a water molecule, which belongs to a water network supporting the active-site geometry. Glu95 Oε2 interacts with another phosphate oxygen (PO_4 O2). Arg120 Nε, Arg120 NH1 and His136 Nε2 are all hydrogen bonded to PO_4 O3. In addition to interactions with the phosphate group, the side chain of Arg120 also makes contacts with loop L4, in which Arg120 NH1 and Arg120 NH2 form hydrogen bonds with Ala119 O and Gly117 O in L4 (Fig. 4). Many main-chain atoms (Ala119 O, Gly117 O, Trp50 O, Gly142 N and Asn140 O) and some water molecules also contribute to the stabilization of the active site.

When the structures of restrictocin and the complex of T1 with 2′-GMP are superimposed, the main-chain and side-chain atoms of Trp47, His49, Glu95, Arg120 and His136 in restrictocin can be spatially aligned with the catalytic residues Trp38, His40, Glu58, Arg77 and His92 in T1 with an rms deviation smaller than 0.1 Å (Fig. 3c). In addition, the phosphorus atom of the inorganic phosphate group in restrictocin is 0.96 Å and 1.21 Å from the phosphorus atoms directly observed in the complex structures of T1 with 2′-GMP and 3′-GMP, respectively [33,34]. These structural data strongly support the identification of the catalytic residues from sequence alignment. Strong conservation in the structural cores and the catalytic residues suggests that restrictocin and T1 share a common catalytic mechanism of RNA hydrolysis, by which the same 3′ phosphate and 5′ hydroxyl groups are produced.

Although the catalytic residues in Sa (Glu54, Arg69 and His85) can also be well aligned with Glu95, Arg120 and His136 in restrictocin, Val35 in Sa lies in the place of His49 in restrictocin (Fig. 3d). As His49 is proposed to serve as the general base in the phosphoryl transfer reaction [38], this discrepancy either argues against the proposed role for His49 in catalysis or suggests a different enzymatic mechanism for Sa.

Table 1

Equivalent structural elements between restrictocin and ribonucleases T1, Ms and F1.

Restrictocin residues	RNase T1 (1rnt)*		RNase Ms (1rds)*		RNase F1(1fut)*	
	Residues	rmsd† (Å)	Residues	rmsd† (Å)	Residues	rmsd† (Å)
3–5	4–6	0.33	5–7	0.29	4–6	0.18
22–34	9–21	1.14	10–22	1.09	9–21	1.03
47–53	38–44	0.30	37–43	0.40	38–44	0.33
68–70	48–50	0.78	47–49	0.69	48–50	0.73
93–99	56–62	0.51	55–61	0.50	56–62	0.53
103–105	66–68	0.27	65–67	0.22	65–67	0.34
115–124	72–81	0.32	71–80	0.27	72–81	0.38
127–136	83–92	0.61	82–91	0.59	83–92	0.59
143–148	99–104	0.62	98–103	0.52	99–104	0.75

*Accession code of the coordinates in the Protein Data Bank. †rmsd is the root mean square deviation between the main-chain atoms (CA,CB, C, N, O) of equivalent structural elements.

The base recognition site

Residues in a ribonuclease which interact with the base 5′ to the cleaved phosphodiester bond are often denoted 'base recognition residues'. Structural alignment of restrictocin with T1 and Sa structures complexed with 2′-GMP or 3′-GMP [33,34,36], identified Phe51, Thr52, Asn53 and Arg65 as the base recognition residues in restrictocin (Fig. 3e). Phe51, Thr52 and Asn53 are located in a type I′ reverse turn (Thr52-Asn53-Gly54-Tyr55) at the start of loop domain L3 of restrictocin; they are in positions comparable to Tyr41, Asn43 and Asn44 (in T1) and Phe37, Gln38 and Asn39 (in Sa). Arg65 of restrictocin comes from a different region of loop L3 and occupies a similar position to Tyr45 in T1 and Arg40 in Sa. As the guanosine-binding site is unoccupied in the crystal structure of restrictocin, Thr52 N, Thr52 Oγ1 and Asn53 O are hydrogen bonded to three water molecules, HOH^{738}, HOH^{875} and HOH^{876}. These four- or five-centered water molecules form a hydrogen-bonding network which supports the geometry of the empty base recognition site in restrictocin (Fig. 3f). It is clear that the active site of restrictocin can accommodate 2′-GMP or 3′-GMP molecules in the conformations and locations observed in the T1 or Sa complexes. N7 and O6 of the guanine base would be located at hydrogen-bonding distance from Thr52 N and Asn53 N, both of which are thought to be key interactions in conferring specificity for the guanine base in T1. N7 and O6 in the guanine base are predicted to be in equivalent positions to HOH^{738} and HOH^{875} in restrictocin. In other words, when 2′-GMP or 3′-GMP bind restrictocin, we predict that only a few hydrogen bonded water molecules will be displaced and that little conformational change will occur in the protein. The base recognition residues of restrictocin are identical to those of Sa yet different from those of T1. Phe51 and Arg65 in restrictocin, and Phe37 and Arg40 in Sa are equivalent to Tyr42 and Tyr45 in T1. Therefore the 'sandwich' effect from the phenolic side chains of Tyr42 and Tyr45 proposed to account for the guanine specificity of T1 [34] might be replaced in restrictocin by stacking interactions of the aromatic ring from Phe51 and the guanidinium group from Arg65.

A very important difference between restrictocin and other ribonucleases is that restrictocin lacks a residue corresponding to Glu46 in T1 or Glu41 in Sa. The branched side chain of this residue forms double hydrogen bonds with N1 and N2 of the guanine base and thereby discriminates guanine from adenine [34,36]. The lack of this residue in restrictocin could explain the observation that

Table 2

Equivalent structural elements between restrictocin and ribonucleases Sa and barnase.

Restrictocin residues	RNase Sa (1gmp)*		Barnase (1bns)*	
	Residues	rmsd† (Å)	Residues	rmsd† (Å)
49–53	35–39	0.92	54–58	0.26
93–98	52–57	0.38	71–76	0.44
119–123	68–72	0.47	86–90	0.31
133	81	0.02	98	0.10
136	85	0.47	102	0.51

*Accession code of the coordinates in the Protein Data Bank. †rmsd is the root mean square deviation between the main-chain atoms (CA,CB, C, N, O) of equivalent structural elements.

Figure 3

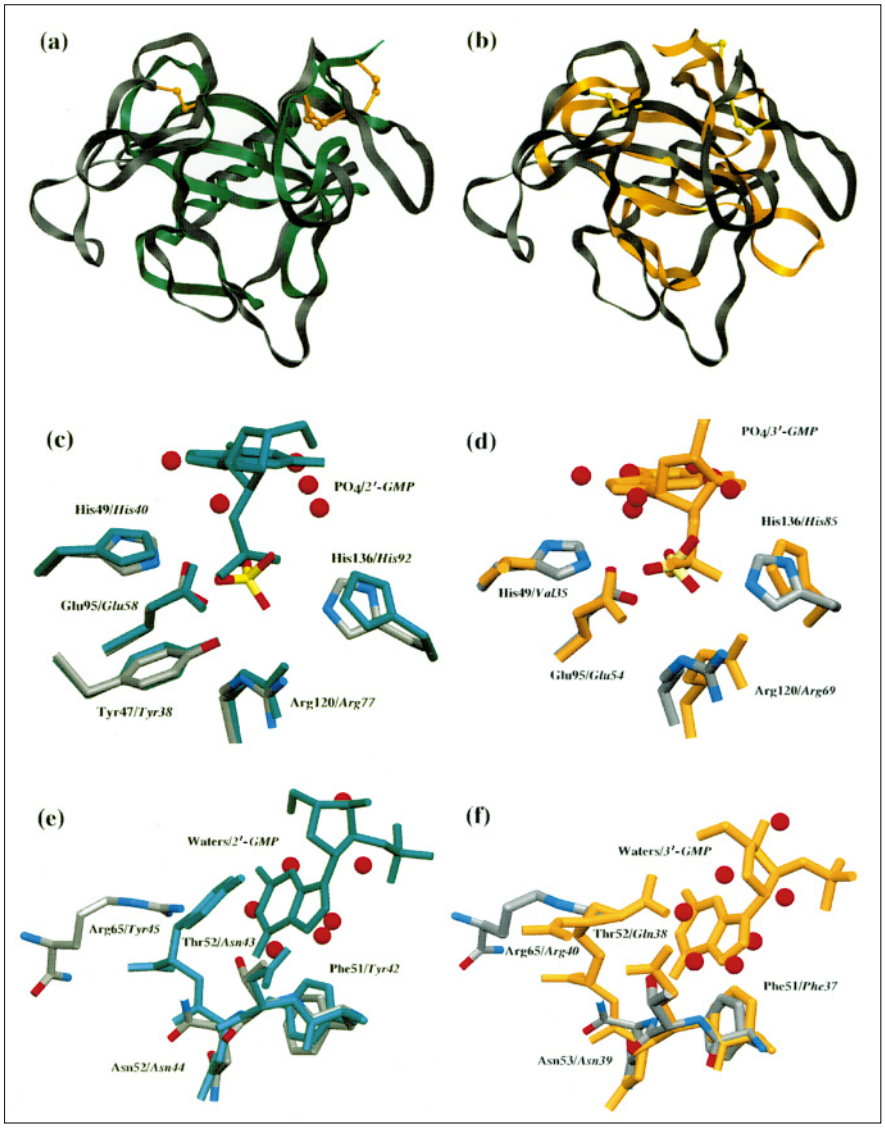

Structural alignment between restrictocin (in gray) and ribonucleases T1 (in green), and Sa (in gold). (a) The overall folds of restrictocin and T1; (b) the overall folds of restrictocin and Sa. (c) The catalytic residues from restrictocin (shown in gray and labeled in plain text) and T1 (shown in turquoise and labeled in italic text). The tetrahedral phosphate group (in red and yellow) is from restrictocin and the 2′-GMP is from T1. Red spheres represent the water molecules in restrictocin. (d) The catalytic residues from restrictocin and Sa (shown in gold and labeled in italic text). The 3′-GMP is from Sa. (e) The base recognition residues of restrictocin and T1, the 2′-GMP is from T1. (f) The base recognition residues of restrictocin and Sa. The 3′-GMP is from Sa. (All six figures produced by the program SETOR.)

restrictocin is only purine-specific towards naked RNAs, rather than guanine-specific as for T1 and Sa [15].

The alignments of the catalytic residues and base recognition residues of restrictocin and other ribonucleases are shown in Table 3. The alignments were derived from their crystal structures, except for U2 [39] and RNase Bi, for which atomic coordinates are not yet available. According to Tables 1,2, ribonucleases with similar folds fall into two major groups: a T1 group and an Sa group. Restrictocin seems to combine the catalytic components of the T1 group with the base recognition components of the Sa group, which reveals the functional relationship between the *Aspergillus* ribotoxins and other ribonucleases. Table 3 also suggests that if these ribonucleases share a common chemical basis for catalysis, His49 might not be directly involved in bond cleavage and Asn53 may play an important role in purine specificity.

The connecting loops

Most of the distinctive structural differences between restrictocin and ribonucleases lie in the peripheral loop regions; differences in loops L3 and L4 are prominent.

Loop L3 (53–91) is the longest loop in restrictocin with two large structural insertions compared to T1. These insertions span residues 52–67 and 69–92 (Fig. 3a,5). The 39 residues in L3 form a structural domain which is absent in other ribonucleases. There are two major interactions between this loop domain and the structural core: a highly solvent-accessible disulfide bond (between Cys75 in L3 and Cys131 in strand B6); and a hydrophobic interaction

between a cluster of residues from L3 (Phe51, Ile68 and Phe70) and the major β sheet (Leu93, Ile122, Val134, Leu144 and Leu146) (Fig. 2b). The secondary structure elements in the L3 domain include a one-turn helix (H2) and several β turns of various types, which fold into four mini-loops. The flexibility of this loop is suggested by the presence of seven glycine residues, but in the crystal lattice L3 is stabilized by extensive intermolecular contacts, which may determine the conformation of the loop. A chain of four ordered water molecules in L3 fills up a gap by interacting with lateral residues (Phe51, Asn53, Ile68, Leu93, Arg77, Cys75 and Asp76). This water chain is found in both molecules of restrictocin in the asymmetric unit, and might help stabilize the loop conformation in the crystal lattice. Three adjacent restrictocin molecules make contacts with L3. At one intermolecular interface, an additional inorganic phosphate group is found. This phosphate group interacts with Arg77 and His91 (from L3) and with the C-terminal residue His149, from the adjacent molecule related by the local 2_1 symmetry. The spatial arrangement of Arg77, His91, His149 and the phosphate group in the interface is very similar to that observed in the active site and corresponds to the positions of the catalytic residues Arg120, His136, His49 and the phosphate group (PO_4). In addition, five lysine and two arginine residues make L3 highly positively charged. Lys60, Lys63, Lys80, Lys88 and Arg65 line up at a ridge that faces towards the entrance to the restrictocin catalytic center. This positioning would allow these residues to move in and interact with the negatively charged phosphate backbone of substrate RNA by forming specific and/or non-specific salt bridges. These interactions might be important in positioning the RNA loop of the substrate towards the active site of restrictocin.

Loop L4 contains five proline residues (Pro97, Pro100, Pro112, Pro116 and Pro118), two at each end, and one at the turn of L4; Gly102 and Gly117 are close to the ends of L4. Compared to T1, in restrictocin there is an eight-residue insertion at the turn of L4 (Fig. 3a), in which four lysine residues are found (Lys106, Lys110, Lys111 and Lys113). This insertion also makes contact with loop L2 at the entrance to the catalytic center. The strategic positioning of the lysine-rich loop (L4) implies a role in substrate-binding and specificity. In the crystal lattice, L4 is very exposed to solvent and its mobility is indicated by significantly higher B factors for the residues in the loop (109–113).

Loop L1 (10–17) links the two N-terminal β strands (Fig. 2a). In the crystal lattice L1 is fully exposed to solvent and lacks electron density for residues 11–16. A loop corresponding to L1 is totally absent in the T1 structure (Fig. 3a). In the sequence of L1, there is a proline residue at the turn and two lysine and two asparagine residues make L1 very hydrophilic. Loop L1 is distant from the catalytic center of restrictocin, and no biochemical

Figure 4

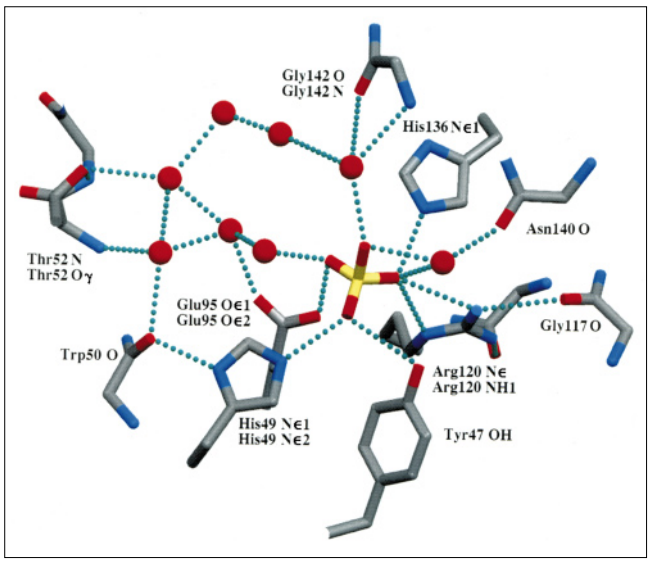

The hydrogen bonding network at the active site of restrictocin. The main-chain and side-chain atoms involved in hydrogen bond formation are labeled. Red balls represent water molecules and the phosphate group is a tetrahedron shown in yellow and red. Turquoise dotted lines represent hydrogen bonds.

data imply its involvement in either interactions with the ribosomal surface or in the ability to enter cells.

Loop L2 (36–48) connects helix H1 and strand B3 in the major β sheet, which is located at the entrance of the catalytic site (Fig. 2a,b). The conformation of L2 is stabilized by internal hydrogen bonds and intermolecular contacts. Residues Lys42, Gly44 and Ser45 located at the turn of L2 make hydrogen bonds with Asp108 and Phe107 in loop L4. In the crystal lattice this interloop interaction is reinforced by Arg21 from the neighboring molecule, whose side-chain atoms are hydrogen bonded with Lys42 O in L2 and Asp108 Oδ1 and Asp108 Oδ2 in L4. The loop–loop interactions between L2 and L4 might lead to the different conformation of L2 in restrictocin from that in T1, despite their identical lengths (Fig. 3a).

Loop L5 is a tight turn of type VIa that links strands B5 and B6. Loop L6 between strands B6 and B7 is a seven-residue loop in which Arg138, Gly139, Asn140 and Gln141 form a type II′ turn. Three ordered water molecules (HOH^{749}, HOH^{721} and HOH^{893}) mediate hydrogen bonding in L6. Although both the length and sequence of L6 are identical to those of T1, L6 in restrictocin is substantially displaced relative to the β strands (Fig. 3a). In L6, Gln137 O and Gly39 N before the turn are hydrogen bonded to Gln8 N, Gln8 O and Asn7 Nδ2 in strand B1; Asn140 O and Gly142 N after the turn interact with the ordered water molecules in the active site (HOH^{718}, HOH^{723} and HOH^{722}). Although the flexibility

Table 3

Structural alignment of the catalytic and base recognition residues in restrictocin and other ribonucleases.

Ribonuclease	Specificity	Catalytic residues	Base recognition residues*	Available structures†
T1	G	Tyr38 His40 Glu58 Arg77 His92	Tyr42–Asn43–Asn44–Tyr45–Glu46	2′GMP; 3′GMP; 2′AMP; free
Ms	G>A>C>U	His37 His39 Glu57 Arg76 His91	Tyr41–His42–Asp43–Tyr44–Glu45	3′GMP
F1	G	Tyr38 His40 Glu58 Arg77 His92	Tyr42–Asn43–Asn44–Tyr45–Glu46	free; 2′GMP
U2	A>G	Tyr38 His40 Glu61 Arg84 His101		n/a
Restrictocin	G or A	Tyr47 His49 Glu95 Arg120 His136	Phe51–Thr52–Asn53 Arg65	PO_4
Sa	G	Arg65 Val35 Glu54 Arg69 His85	Phe37–Gln38–Asn39–Arg40–Glu41	3'GMP; 2'GMP
Barnase	G	Arg83 Asp54 Glu73 Arg87 His102	Phe56–Ser57–Asn58–Arg59–Glu60	free; d(GpC); barstar
St	G	Arg72 Thr42 Glu61 Arg76 His91	Phe44–Glu45–Asn4–Arg47–Glu48	SO_4
Bi	G	Arg82 Asp53 Glu72 Arg86 His101	Phe55–Ser56–Asn57–Arg58–Glu59	n/a

*Base recognition residues refer here to those residues interacting with the base in substrate RNA that is located 5′ to the phosphodiester bond to be cleaved. †Several crystal structures are available for many of the aligned ribonucleases both in free and complexed forms, the types of complex are listed. Barstar is a small protein inhibitor of barnase.

of L6 would be facilitated by Gly139 and Gly142, Asn7 and Gln8 are likely to be responsible for the displacement of the loop as these residues are absent in the T1 structure. The different loop conformations of L6 in the restrictocin and T1 crystal structures may simply represent two selections of many possible conformations for a flexible loop.

Surface properties

The molecular surface of restrictocin reveals a dome-shaped protein with the active site located on the planar side (Fig. 5a,b). Looking down on the active site , the catalytic residues are located at one end of a shallow cleft, which is extended by a large platform at the entrance formed by loops L2 and L4 (Fig. 5a). The platform is about 20 Å wide, limited by loops L3 and L6 as the boundary. It is plausible that the concave surface of the platform is the surface in restrictocin that binds the substrate RNAs. The surface of restrictocin is highly positively charged, which is consistent with its very basic isoelectric point (*pI*~9.0) established by isoelectric focusing gels (XY, unpublished result). Most charges are uniformly distributed over the surface except in two regions where positive charges are concentrated. One region is the lysine-rich loop in L4 which looks like a knob at the edge of the platform (Fig. 5a,b). The other region is the positively charged ridge in L3 (containing Lys60, Lys63, Lys80, Lys88 and Arg65) that faces towards the platform. The locations of the two clusters of positively charged residues also supports the idea that the platform, formed by L2 and L4 at the entrance of the catalytic site, is the extended binding site of substrate RNA.

Although restrictocin and T1 bear limited sequence and structural identity, major differences in the peripheral loops lead to very different molecular surfaces. As it lacks the loop domain L3, T1 does not adopt a dome shape. There is no platform at the entrance of the active site of T1 because loop L4 is much shorter and L3 is in a very different conformation. The lysine-rich knob and the positively charged ridge inserted in restrictocin are absent in T1 and make the catalytic center of T1 more accessible. This comparison suggests that the structural elements responsible for restrictocin substrate RNA binding are a landing platform (L2 and L4), a lysine-rich loop (L4) and a positively-charged ridge in loop domain L3.

Crystal packing

There are two restrictocin monomers in one asymmetric unit related by a non-crystallographic twofold screw axis. In the crystal lattice one restrictocin monomer (model A) contacts four adjacent molecules (model B) related by crystallographic symmetry: B0 (x, y, z); B1 (1–x, y+1/2, 1–z); B2 (–x, y+1/2, 1–z); and B3 (x, y, z+1). Most interactions at the interfaces are salt bridges between polar or charged side chains. These are either direct interactions or mediated by solvent molecules like waters or phosphate groups. Two pairs of stacking interactions are formed between an imidazole ring and an arginine guanidinium group, His103A–Arg85B and His35A–Arg138B, in interfaces A0–B1 and A0–B2. Due to the non-crystallographic symmetry, the four interfaces fall into two types. A0–B1 and A0–B2 are type I interfaces; A0–B0 and A0–B3 belong to type II. Type I interfaces form a concave/convex fitting between the active-site residues of one molecule and residues from adjacent molecules (Lys28, Ser31 and His35 in H1; Asp101, Gly102, His103, Asp104, Lys113 and Asn115 in L4). In the crystal lattice the active sites of both molecules in the asymmetric unit are blocked to the point where even a mononucleotide cannot readily diffuse in (C Dealwis, unpublished results). The interfaces related by non-crystallographic symmetry also differ in some chemical details. One interesting example is that two heavy-atom ions (Hg^{2+}) bind His91A and His149B at one of the type I interfaces but not the other, where instead a phosphate group interacts with His91B and His149A. It is

unlikely that either interface represents a biologically relevant dimer association. A trace band of restrictocin dimer was observed in SDS-PAGE gels run under reducing conditions [23]. This observation might be due to random reassociation of disulfide bonds between molecules; no biochemical evidence suggests that the *Aspergillus* ribotoxins function as dimers *in vivo*. These intermolecular interfaces may simply reflect the way that the restrictocin molecules pack in this $P2_1$ space group under our crystallization conditions.

Discussion

Catalytic mechanism

Structural comparisons of restrictocin with other ribonucleases reveal a T1-like structural core responsible for the purine-specific ribonuclease activity of restrictocin. The catalytic residues of restrictocin are identified as His49, Glu95, Arg120 and His136. The high conservation of sequence and tertiary structure, especially around the catalytic center, strongly suggests that restrictocin shares its catalytic mechanism with T1. Yang and Kenealy [40] constructed three point mutants of restrictocin, Glu95→Gly, Glu115→Gly/His136→Leu and His136→Leu to test this hypothesis. Using an *in vivo* yeast system and an *in vitro* translation assay, they found that Glu95→Gly was partially active while Glu115→Gly/His136→Leu mutants lost their toxicity towards the host cells. This result suggests the direct involvement of His136 in restrictocin catalysis.

Based on studies of T1 [33–35], we propose a two-step reaction mechanism for restrictocin catalysis involving a phosphoryl transfer reaction and a hydrolysis reaction. In the phosphoryl transfer reaction step, His49/Glu95 in restrictocin serves as the general base to abstract a proton from the 2′OH of ribose; His136 acts as the general acid to protonate the O5′ atom of the leaving nucleotide (product 5′OH), resulting in formation of a 2′-3′ cyclic phosphate intermediate. The phosphorus atom of inorganic phosphate in the restrictocin structure is almost equidistant from the O2′ and O3′ atoms of 3′-GMP in the T1 structure, within the restrictocin/T1 structure alignment. This phosphate might represent the position of the actual phosphorus atom in the 2′-3′ cyclic phosphate intermediate. In the hydrolysis reaction, the roles of the catalytic residues are reversed; His136 works as the general base to activate a water molecule and His49/Glu95 protonates the O2′ atom. The activated water molecule then attacks the phosphorus atom in the intermediate and forms the second product 3′ phosphate. No water molecule has been found in the restrictocin model that corresponds to the proposed activated water. The role of Arg120 is less clear. It may stabilize the phosphate group through electrostatic interactions or support the active-site geometry for the proper positioning of the catalytic residues by forming extensive hydrogen bonds (Fig. 4). Although Tyr47 contributes to the hydrogen-bonding network of the active site, and structurally can be very well superimposed with Tyr38 of T1, its role in catalysis is not known.

Figure 5

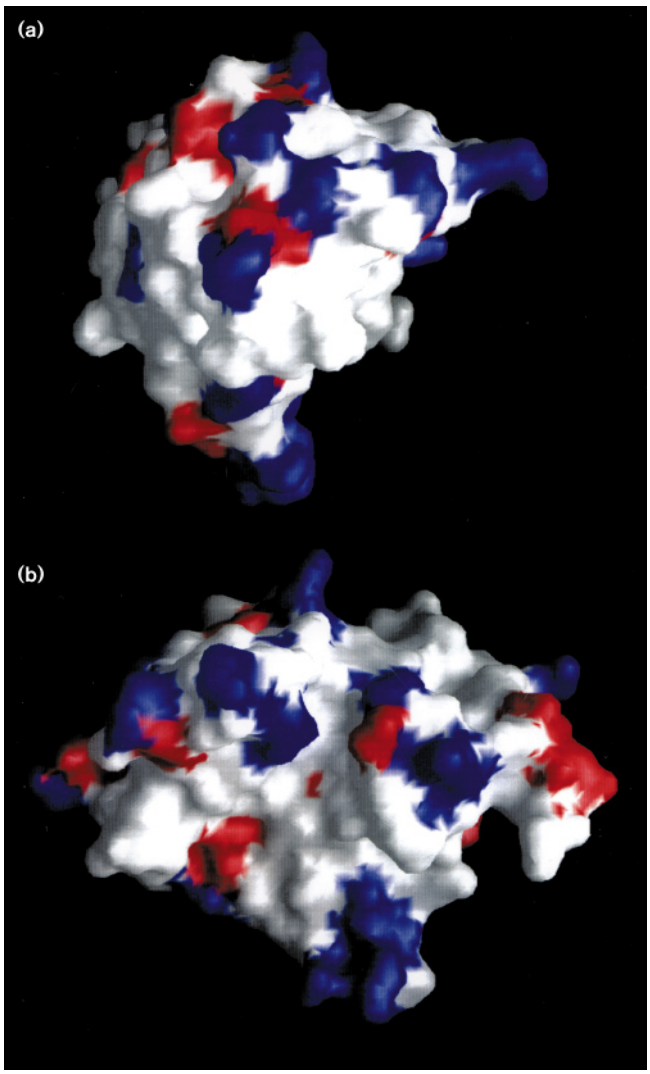

Charge distribution on the surface of restrictocin. Positive charges from lysine and arginine residues are in blue; negative charges from aspartic acid and glutamic acid residues are in red. (a) The figure shows a dome-shaped restrictocin surface with the active site located at the planar side. (b) A charge distribution surface with a view looking down at the active site. Two major clusters of positive charges are revealed around the active site: a long ridge from loops L3 and L6; and a knob in loop L4 that is rich in lysines. (Surfaces are generated and displayed with the program GRASP [65].)

Identification of the general base and general acid in the catalytic mechanism of T1 is not unambiguous. Heinemann and Saenger [33] proposed a mechanism in which Glu58 and His92 act as general base and general acid respectively. The mechanism was based on the crystal structure of T1 complexed with 2′-GMP and on early spectroscopic and kinetic studies. This model was challenged

by Nishikawa *et al.* [41], who observed high residual activity in the T1 mutant Glu58→Ala. They proposed a different mechanism in which two histidines (His40 and His92) act as a base-acid couple, as in the case of bovine pancreatic ribonuclease A [42]. Evidence from a study of the pH dependence of catalysis in a series of T1 mutants [43] suggests that the Glu58/His92 pair represent the required base-acid couple and that His40 electrostatically stabilizes the 2′-3′ cyclic phosphate intermediate. Our structural comparison of restrictocin with T1 and Sa supports the Glu58/His92 base-acid couple hypothesis. As T1 and Sa have very similar overall folds and active-site geometry and both are purine-specific, it is very likely that they employ the same catalytic mechanism. Alignment of Val35 (Sa) with His40 (T1) and His49 (restrictocin) may simply indicate a non-essential role of His49 in restrictocin catalysis.

The base recognition site

Structural alignments of restrictocin with T1 and its various complexes indicate that in the active site and base-recognition regions, the restrictocin structure mimics T1 structures complexed with 2′-GMP or 3′-GMP more closely than those complexed with vanadate, 2′-AMP or the free enzyme [35,44,45]. In the free T1 structure or in complexes with vanadate or 2′-AMP, an internal hydrophobic residue, Val78, is found in two conformations; when the guanine-recognition site is occupied in T1 complexes with 2′-GMP, 3′-GMP, 2′5′-GpG and 3′5′-pGp this residue is well-ordered. In restrictocin, the active site is bound only by a phosphate group from the crystallization buffer and the counterpart residue, Val121, shows very well-defined, ordered density. For the base-recognition residues (Fig. 3d), in contrast to Asn43N in the free T1 structure, which points away from Guanine O6, Thr52N in restrictocin points towards Guanine O6 in the alignment as does Asn43 N in the T1–2′-GMP or T1–3′-GMP complex structures. This suggests that the subtle structural changes in T1 upon GMP binding, such as the 140° flip of the Asn43-Asn44 peptide plane in T1 [35], might be initiated by binding of the phosphate group at the catalytic site. This binding then propagates to the base-recognition region, and helps reinforce the interactions between restrictocin and bases in the substrate RNA. Whether similar conformational changes would happen in the base-recognition site of restrictocin upon substrate binding will not be known until the crystal structures of free restrictocin and restrictocin–RNA complexes are solved.

Docking experiments and substrate specificity

One of the most intriguing features of restrictocin is its high substrate-specificity. Based on this restrictocin crystal structure and the NMR structure of a 29-mer substrate RNA analog, denoted E73 [46], we have built a preliminary docking model. The model aims to identify the structural elements responsible for substrate-specificity and specific interactions between protein and substrate RNA.

The conformation of E73 reveals a compact structure with several purine–purine base pairs, a GAGA tetraloop and a bulged guanosine adjacent to a reverse Hoogsteen AU pair (Fig. 6a). Based on this E73 structure, a large number of 35-mer variants were made in order to define the critical elements for specific recognition by α-sarcin of the substrate [17]. In order to retain substrate specificity, several features are required: G18 in the 35-mer (G16 in E73) at the cleavage site is preferred but can be replaced by any other base; G12 (corresponding to the bulged G10 in the E73 NMR structure) cannot be deleted or mutated; a stem with a minimum of two base pairs is required to tether the loop; and the GAGA tetraloop is preferred, but it alone as a miniloop is not sufficient for specific recognition [16]. These results suggest an important role for the tertiary structure of the substrate RNA in protein–RNA specific recognition.

Surface curvature calculated by the program GRASP reveals a concave surface near the catalytic site in the dome-shaped restrictocin (Fig. 5a,b). As expected for an RNA-binding site, this concave surface is populated with basic residues, including a lysine-rich region at the turn of loop L4 and basic residues lining up at the edge of loop L3. With the help of the program GRASP, the following constraints were applied in our docking experiment: surface complementarity between the concave surface of restrictocin and the loop head of E73; and the protruding lysine-rich knob fitting into the major groove of the helical stem of the RNA. Suggestively, the resultant model of the complex locates the phosphorus atom at the cleavage site (between G16 and A17) of E73 only 0.93 Å away from the phosphate group in the restrictocin crystal structure (Fig. 6a). In this docking model, the platform formed by loops L2 and L4 provides the major interaction interface with E73. Lys42 in L2 and Lys110-Lys111-Pro112-Lys113 in L4 are in positions that could stabilize interactions with the backbone of E73 by forming salt bridges with negatively charged phosphates. The side chains of Asp108 or Ser109 may form hydrogen bonds with donor/acceptor atoms in bases of the substrate and function as base discriminators. The positively charged ridge, formed by Lys60, Lys63, Lys80, Lys88 and Arg65, in loop L3 is close to the sugar-phosphate backbone of G13–G16 in E73. The ridge in L3 might be extensively involved in protein–RNA interactions. In addition, the van der Waals surfaces of restrictocin and E73 fit each other very well with a solvent-excluded surface area of 870 $Å^2$ (Fig. 6b).

Although the current docking model is still preliminary, it provides interesting insights into the interactions between restrictocin and E73. Firstly, G10 in E73 is known to be a base essential for the substrate-specificity [17]. In our model, G10 is close to the lysine-rich loop in L4 (Fig. 6a). Consistent with this interaction, a deletion in the

Figure 6

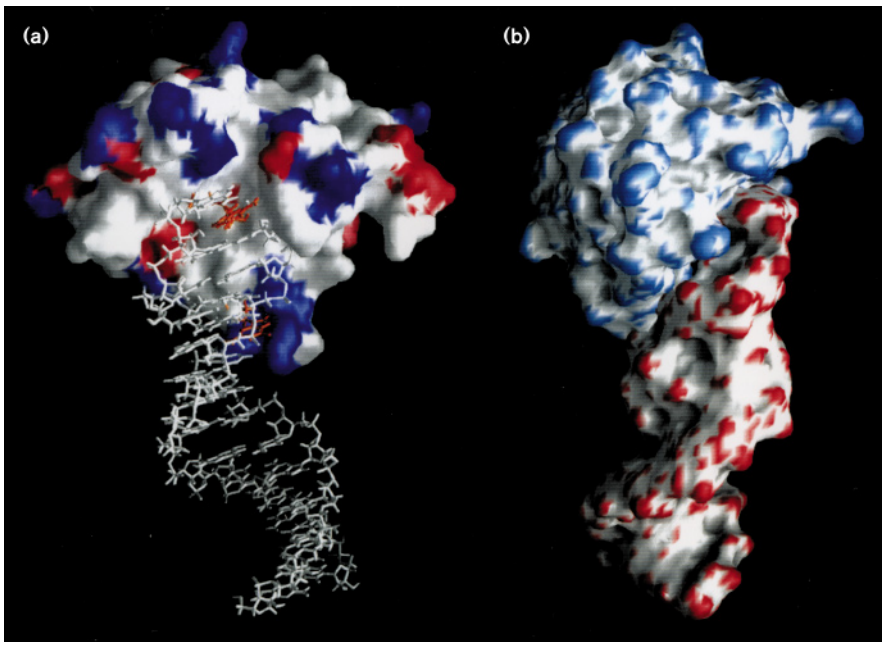

A docking model derived from the restrictocin crystal structure and the NMR structure of a 29-mer RNA substrate analog (E73). (a) The figure shows the positioning of the bulged guanosine residue (G10) and G16 (both in gold) at the cleavage site of E73 (in gray) with respect to the charge distribution of restrictocin. (b) The surface complementarity between restrictocin and E73 shown in a 90° view from that of (a). Surfaces, where the surface curvature calculated by GRASP is positive, are shown in blue and red for restrictocin and E73, respectively.

lysine-rich loop (106–113) of restrictocin leads to loss of substrate specificity (R Kao, J Davies, [abstract VII-5], International Conference on the Structure and Function of the Ribosome, Victoria, BC, Canada, May 1995). The specific recognition between G10 and the lysine-rich loop might be one of the key interactions responsible for the substrate specificity. Single mutants in the lysine-rich region could further identify key residues and the types of interaction involved. Secondly, the phosphate group at the cleavage site of E73 (A17) is in a very good position to interact directly with the catalytic residues of restrictocin (Fig. 6a). Glück and Wool [17] showed that a two-base insertion between the cleavage site and the bulged G10 of E73 resulted in a two-base shift of the cleavage site; they suggested the existence of a molecular ruler between the active site and the specific recognition region, such as G10 in E73. Finally, by comparisons with other ribonuclease structures, complexed with 2′- or 3′-GMPs, we identified a base-recognition site in restrictocin (Fig. 3e,f). The base-recognition site is empty in this docking model, probably because both components of the model (restrictocin and E73) are assumed to be rigid. In addition, the GAGA (14–17) tetraloop in the E73 NMR structure is folded in a closed conformation with A15, G16 and A17 stacking together and base pairing between G14 and A17. It is possible that when restrictocin binds to E73, the GAGA tetraloop will open up so that G16 could be properly positioned in the base-recognition site of restrictocin and interact with the base-recognition residues, Phe51, Thr52 and Asn53. This conformational change is compatible with the positioning of the GAGA tetraloop in the current docking model.

Loop domain L3 and cell-entry activity

As a ribotoxin, restrictocin has the ability to enter cells, a property which related ribonucleases such as T1 lack. However, unlike ricin for which the B chain facilitates entry of the catalytic A chain into cells [47], restrictocin is a single chain ribotoxin that apparently translocates across the cell membrane without the involvement of other proteins. Although the *Aspergillus* ribotoxins have shown very limited cell-entry activity against intact cells *in vitro*, they can enter virus-infected cells and many tumor cell lines. When the *Aspergillus* ribotoxins were tested as antitumor drugs, they were proved to be toxic [14], suggesting that restrictocin can also get into normal cells and attack their ribosomes. What structural elements in restrictocin might be responsible for its cell-entry activity?

The structural feature in restrictocin which distinguishes it most from T1 is the large 39-residue loop (L3) between β strands B3 and B4 that forms an extra loop domain in restrictocin. There are no secondary structure elements in L3 except for an α helix with a single turn. A disulfide bond in L3 splits the loop into two topological loops. The loops stretch out in a direction perpendicular to the connecting strands, which looks like a ship anchor (Fig. 7a). Before the crystal structure of restrictocin was known, it was thought that this loop might be responsible for the specific recognition of substrate RNAs (J Smith, personal communication). However, neither the free restrictocin structure nor the docking model for the restrictocin–RNA complex indicates direct and essential involvement of loop L3 in the specific recognition. From the structural analysis of restrictocin, we speculate that the loop domain

L3 might be related to the cell-entry ability of restrictocin. Interestingly, similar large loop conformations are also found in the sugar-binding domains of some lectin structures, such as ricin B chain [48,49], rat mannose-binding protein (MBP) [50] and some plant lectins [51,52]. Ricin B chain consists of six copies of a galactose-binding motif, which contains 40 residues closed by two adjacent antiparallel β strands. It is believed that the ricin B chain can bind reversibly to galactose residues presented by cell surface glycopeptides and/or glycolipids and facilitates the uptake of the whole molecule of ricin (A and B chains) by endocytosis [48,49]. Significantly, this loop is topologically similar to the loop domain L3 of restrictocin (Fig. 7b). Other proteins are known to contain similar large loops: the calcium-dependent lectin domain of a rat MBP, lectin-like domain in CD69, E selectin, lectin-homology domain in murine IgE receptor and P-selectin (CD62) (Fig. 7c). Divalent ions such as Ca^{2+} and/or Mg^{2+} are ligated in these loops, and involvement of the loops in sugar-recognition has been implied by mutational studies [50,53–55]. As in restrictocin, these loops form independent loop domains; they often consist of four small loops lacking regular secondary structure elements and the loops are closed by an adjacent antiparallel β strand. Plant lectins with similar loops in sugar-binding domains include lentil lectin, legume isolectins I and II, pea lectin and peanut lectin [51,52] (Fig. 7d). These plant lectins share similar β sandwich tertiary folds. Divalent ions (Ca^{2+} and Mg^{2+}) and carbohydrate bind large loops clustered at one side of the β sandwich. Although these large loops are topologically similar, similarity in their primary sequences is poor and tertiary structural alignment of these loops does not seem very satisfactory. This is not surprising, as loops involved in cell surface recognition, such as those in heavy chain variable regions of immunoglobin structures, may confer their specificity by adopting different tertiary conformations.

In order to understand the cell entry mechanism of α-sarcin, Gavilanes and colleagues have studied the interactions between α-sarcin and lipids using model membrane systems and several tumor cell lines. They have shown that α-sarcin interacts with phospholipid vesicles and promotes their aggregation and fusion [25,26]. The secondary structure of α-sarcin seems to be modified upon interactions with acid phospholipids or detergents like sodium dodecylsulfate (SDS) [26]. α-Sarcin can penetrate the lipid bilayer of tRNA-containing asolectin liposomes and degrade entrapped tRNAs, or be itself degraded by encapsulated

Figure 7

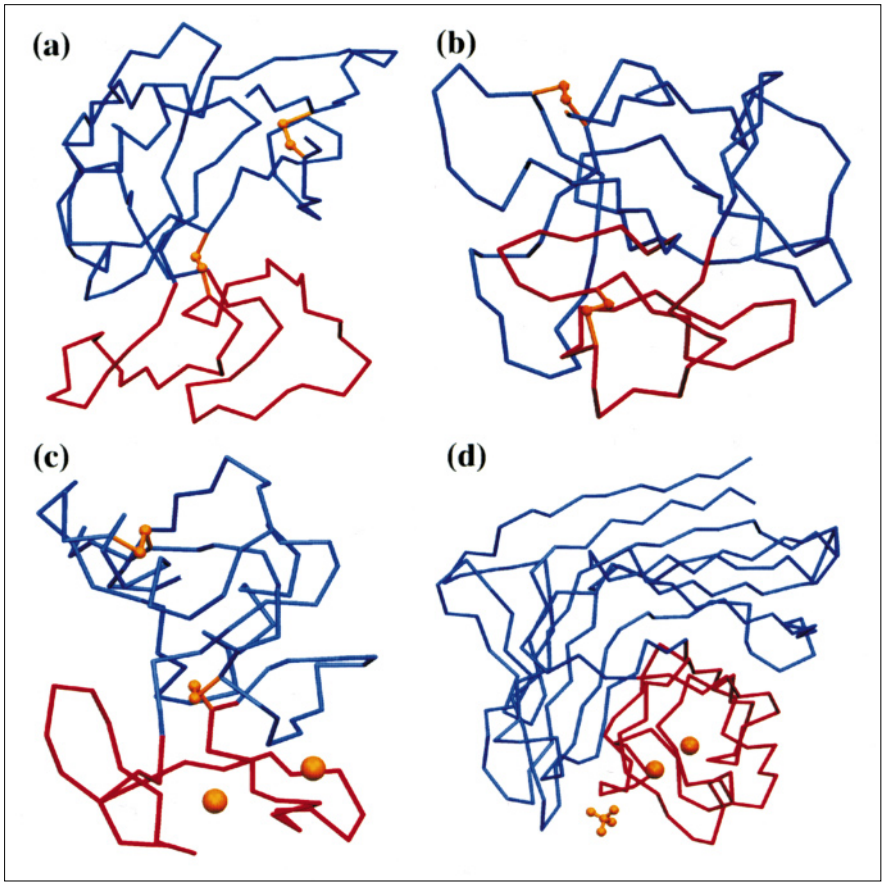

Comparison of loop domains (in red) in restrictocin and other sugar-binding proteins. The loop domains of four proteins are compared: (**a**) restrictocin; (**b**) one domain of ricin B chain; (**c**) rat mannose-binding protein (MBP); and (**d**) lentil lectin, as an example of a plant lectin. Disulfide bonds are shown in yellow. The yellow spheres represent cation-binding sites and the tetrahedron a phosphate-binding site.

trypsin [27]. Extracellular α-sarcin can enter tumor cells and inhibit protein synthesis in the absence of any other agents affecting membrane permeability [23]. Kinetic analysis of this inhibition revealed an α-sarcin-concentration dependent lag phase followed by a first order decrease of the protein synthesis rate. These studies all suggest a translocation mechanism that involves protein–lipid interactions, which might also be rate-limiting in *in vivo* cytotoxic actions.

Loop L3 in restrictocin might recognize sugars in cell surface glycolipids or glycopeptides and thereby promote the endocytosis of restrictocin. Alternatively, the positively charged residues in L3 interact with negatively charged phospholipids in cell membranes, as observed with an *in vitro* model membrane system [25]; this interaction induces an aggregation and fusion of the membrane that helps restrictocin molecules get into the cell.

Biological implications

Restrictocin is a highly specific ribotoxin that cleaves a single phosphodiester bond in rRNA out of 7000 such bonds in eukaryotic 28S ribosomes. The cleavage site is located within a highly conserved purine-rich sequence, which is also the binding site for elongation factors. Many biochemical and mutational studies have been carried out on both ribotoxins and RNA substrate analogs. However, the molecular basis for the catalytic mechanism, substrate specificity and how the ribotoxins get into cells are not understood. Here we report the crystal structure of restrictocin at 1.7 Å resolution, the first structure determined of a member of the *Aspergillus* ribotoxin family. Structural comparison with other ribonucleases reveals an RNase T1-like structural core in restrictocin that is responsible for its ribonuclease activity via an identical catalytic mechanism. A distinctive feature of the restrictocin structure is large flexible loops which join secondary structure elements of the structural core. Two loops at the entrance of the active site form a platform that might specifically recognize substrate RNAs. A lysine-rich segment in loop L4 and a positively charged ridge in loop domain L3 are also implicated in the binding of substrate RNAs. The loop domain L3 may also function as an anchor for the membrane translocation of restrictocin. This crystal structure will guide biochemists and molecular biologists in their studies of the *Aspergillus* ribotoxins, in order to understand protein–RNA specific interactions, develop therapeutic immunotoxins and explore pathogenic mechanisms of *Aspergillus* related human diseases.

Materials and methods

Crystallization

A combination of vapor diffusion and microdialysis techniques were used to crystallize restrictocin [56]. The two-step equilibration greatly slows down the growth rate of crystals and proved to be essential to obtain large crystals of restrictocin. The final mother liquor consists of 60% ethanol, 10 mM sodium phosphate at neutral pH 6.8 and 10 mg ml^{-1} restrictocin. Crystals form long rods in one week with a typical size of 0.3 x 0.3 x 0.8 mm. These crystals can diffract up to 1.6 Å resolution with a laboratory X-ray source and up to at least 1.4 Å on Laue images collected at the NSLS X26C beamline [57]. Precession photos show that restrictocin crystals are in $P2_1$ space group with cell dimensions a = 50.24 Å, b = 82.16 Å, c = 38.04 Å and β = 100.5. This cell is closely similar to that of mitogillin [56]. There are two molecules of restrictocin per asymmetric unit with a solvent content of about 46%.

Data collection and SIRAS phasing

The $HgCl_2$ derivative crystals were produced by soaking native crystals in a solution containing 0.1 mM $HgCl_2$, 10 mM sodium phosphate and 67% ethanol for about 36 h. Native and $HgCl_2$ derivative data sets used in primary phasing were collected on an in-house Enraf Nonius FAST area detector. Reflections for each scan were indexed and integrated by the programs *MADNES* and *PROCOR*. Individual scans were then scaled and merged by monochromatic scaling algorithms in the program *LaueView*, including isotropic scaling factor, isotropic temperature factor, anisotropic scaling factor and anisotropic temperature factors [58–60]. To complete an anomalous data set, two crystals of the $HgCl_2$ derivative were used. Both isomorphous and anomalous difference Patterson maps are of excellent quality; they are the key to our successful structure determination by single isomorphous replacement and anomalous scattering (SIRAS) techniques. Initial heavy-atom positions were refined by the program *Xheavy* in the *XtalView* suite [61]. SIRAS phases at 2.1 Å resolution were then calculated by *PHASES*, followed by 16 cycles of solvent-flattening and yielded a final figure of merit 0.884. Data collection and phasing statistics are shown in Tables 4 and 5. The initial atomic model was built using the program *Xfit* in the *XtalView* suite against the figure of merit weighted Fo (fom*Fo) SIRAS map at 2.1 Å resolution.

The self-rotation function of the native data set of restrictocin, calculated by *POLARRFN* in the *CCP4* program suite [62], reveals two peaks at k = 180°. One of the non-crystallographic twofold axes lies along the a axis, which, in combination with the perpendicular crystallographic 2_1 b axis, generates the third non-crystallographic axis along c*. The packing of restrictocin monomers in real space reveals translations associated with each non-crystallographic twofold axis and suggests a

Table 4

Data collection statistics.

Data set	Native	$HgCl_2$ (isomorphous)	$HgCl_2$ (anomalous)
Number of crystals	2	2	2
Resolution (Å)	15.0–2.0	15.0–2.0	15.0–2.0
Number of unique reflections	18 989	18 567	35 848
Mean redundancy	5.32	6.39	3.31
Completeness (%)			
15.0–2.2 (Å)	99.3	99.2	96.0
2.2–2.1 (Å)	92.5	94.5	81.1
R_{merge}* (%)	3.52	5.16	5.16
$R_{difference}$† (%)			
15.0–2.5 (Å)	_	19.1	7.9

*$R_{merge} = (\Sigma_{hkl} \Sigma_i|I_i - I|) / (\Sigma_{hkl} \Sigma_i (I_i))$, where I_i is one measurement of a unique reflection hkl and I is the mean of all the measurements for the reflection hkl. †$R_{difference} = \Sigma_{hkl} ||F_1| - k|F_2|| / \Sigma_{hkl} |F_1|$, where k is a scale factor. The summation is over all common reflections of two data sets. For the isomorphous difference, F_1 and F_2 represent structure factors from the native and derivative data sets. For the anomalous difference, F_1 and F_2 are the structure factors for a Friedel pair (F^+ and F^-).

pseudo-$P2_12_12_1$ symmetry in restrictocin crystals. The two monomers in the asymmetric unit were independently traced; molecular averaging by *Xfit* was only applied in model building where ambiguity in chain tracing occurred.

Laue data collection and structure refinement

The 1.7 Å resolution Laue data set was reduced from 62 Laue images collected at the X26C beamline of the National Synchrotron Light Source (NSLS) at Brookhaven National Laboratory. The exposure time for the first 31 Laue images was 0.5 ms; for an additional 31 images a 10 ms exposure time was used to enhance high-resolution reflections. The total exposure time was about 325 ms. Laue data reduction was carried out by the program *LaueView*, including both singles and deconvoluted multiples after wavelength normalization and harmonic deconvolution [58,59] (Table 6). Detailed Laue data collection and reduction stategies will be reported in a separate paper (XY, unpublished data). The model was refined against both the FAST data at 2.0 Å resolution and then Laue data at 1.7 Å resolution with protocols in the X-PLOR package, alternating with manual model rebuilding against (2Fo–Fc) and (Fo–Fc) maps by *Xfit*. This is the first time, to our knowledge, that a complete set of high-resolution synchrotron Laue data was used in the conventional refinement of a new structure. This example demonstrates the potential of the Laue method for routine, high quality data collection at synchrotron beamlines, in addition to its long recognized advantages in data collection speed and in time-resolved crystallographic studies.

Structure analysis

The stereochemistry of the restrictocin model was checked with *PROCHECK* [63]. A Ramachandran plot showed that 92% of the residues in the two independent monomers lie in the most favored region and none in disallowed regions. The real space correlation coefficients were examined as a function of residue number, as implemented in the program *O* [64]. Tertiary structural alignments with other ribonucleases were carried out using the programs *LSQKAB*, *COMPAR* in the *CCP4* suite of programs and *Xfit* in *XtalView*. The charge distribution surface and surface curvature of restrictocin were calculated and displayed by the program GRASP [65].

Table 5

SIRAS phasing statistics at 2.1 Å resolution.

	$HgCl_2$ isomorphous	$HgCl_2$ anomalous
Resolution (Å)	15.0–2.1	15.0-2.1
$R_{centric}$*	0.52	
$R_{anomalous}$†		0.37
Mean phasing power‡	2.70	2.83
Isomorphous phasing power at highest resolution bin (2.24–2.10 Å)	1.86	
Anomalous phasing power at highest resolution bin (2.30–2.10 Å)		1.50
Mean figure of merit#	0.72	

*$R_{centric} = \Sigma ||F_{PH}\pm F_P|–k|F_H calc|| / \Sigma |F_{PH}\pm F_P|$, where k is a scale factor. The summation is for centric reflections only. †$R_{anomalous} = [\{\Sigma(|\Delta F^{\pm}obs|–|\Delta F^{\pm}calc|)^2\} / \{\Sigma(\Delta F^{\pm}obs)^2]^{1/2}$, where $\Delta F^{\pm}$ is the structure-factor amplitude difference between Friedel pairs. ‡Phasing power = $(\Sigma|F_H|^2 / \Sigma|E|^2)^{1/2}$, where $\Sigma|E|^2 = \Sigma\{|F_{PH}obs|–|F_{PH}calc|\}^2$. The summations are made over all the reflections observed for the derivative. #Figure of merit = $|F(hkl)_{best}| / |F(hkl)|$ for a reflection (hkl), where $F(hkl)_{best} = \Sigma P(\alpha)F_{hkl}(\alpha) / SP(\alpha)$. The mean figure of merit was calculated for 13 598 phased reflections. The summations are made over all the possible phase angles (α); $P(\alpha)$ is the probability for a reflection F(hkl) to take a phase angle α.

Table 6

Structure refinement statistics against synchrotron Laue data at 1.7 Å resolution.

Data collection	62 Laue images collected at the NSLS X26C beamline
R_{merge} (unweighted/weighted)* (%)	8.2 / 3.9
Redundancy	8.0
Resolution range (Å)	8.0–1.7
Number of observations (after 2σ cut-off)	28328
Number of non-hydrogen atoms	2492
R factor (%)	17.7
Free R factor (%)	23.7
rms deviations from ideal stereochemistry	
Bond length (Å)	0.018
Bond angle (°)	2.02
Dihedral angle (°)	27.1
Average B factors (Å^2)	
Main chain	19.9
Side chain	20.8
Average rms deviations of B factors (Å^2)	
Main chain	1.5
Side chain	6.9

*$R_{merge} = \Sigma_{hkl}\Sigma_i(w_i|F_i–F|)/\Sigma_{hkl}\Sigma_i(w_iF_i)$, where F is the weighted average of structure factors F_i for a unique reflection (hkl). For unweighted R_{merge}, $w_i=1$; for weighted R_{merge}, $w_i=1/\sigma_2(F_i)$.

Accession number

The atomic coordinates will be deposited in the Brookhaven Protein Data Bank.

Acknowledgements

We thank Dr William Kenealy, originally of the University of Wisconsin at Madison and now at J Whittier Biologics Inc. of Madison, Wisconsin, who purified the restrictocin used for these studies. We thank Dr Sergio Martinez and Professor Janet Smith of Purdue University for providing the restrictocin, helpful advice on its crystallization and heavy atom derivative preparation, and discussions on the results. We are grateful to Dr Zhong Ren for his advice, discussion and help in structure determination and refinement. We also thank Drs YL Chan, Anton Glück, Alex Munishkin and Ira Wool for helpful discussions on the biochemical studies on restrictocin, and Dr Chris Dealwis for his initial studies on the complexes of restrictocin and oligonucleotides. This work is supported by grants from NIH to KM and by NIH grant GM 52706 to Dr William Kenealy.

References

1. Schindler, D.G. & Davies, J. (1977). Specific cleavage of ribosomal RNA caused by alpha sarcin. *Nucleic Acids Res.* **4**, 1097–1110.
2. Roga, V., Hedeman, L.P. & Olson, B.H. (1971). Evaluation of mitogillin (NSC-69529) in the treatment of naturally occurring canine neoplasms. *Cancer Chemother.* **55**, 101–113.
3. Gavilanes, J., Vazquez, D., Soriano, F. & Mendez, E. (1983). Chemical and spectroscopic evidence on the homology of three antitumor proteins: α-sarcin, mitogillin and restrictocin. *J. Protein Chem.* **2**, 251–261.
4. Rodriguez, R., Lopez-Otin, C., Barber, D., Fernandez-Luna, J.L., Gonzalez, G. & Mendez, E. (1982). Amino acid sequence homologies in α-sarcin, restrictocin and mitogillin. *Biochim. Biophys. Res. Commn.* **108**, 315–321.
5. Chan, Y.L., Endo, Y. & Wool, I.G. (1983). The sequence of the nucleotides at the α-sarcin cleavage site in rat 28S ribosomal ribonucleic acid. *J. Biol. Chem.* **258**, 12768–12770.
6. Furutani, M., Kashiwagi, K., Ito, K., Endo, Y. & Igarashi, K. (1992). Comparison of the modes of action of a vero toxin (a Shiga-like toxin) from *Escherichia coli*, of ricin, and of α-sarcin. *Arch. Biochem. Biophys.* **293**, 140–146.

7. Lin, A., Chen, C.K. & Chen, Y.J. (1991). Molecular action of tricholin, a ribosome-inactivating protein isolated from *Trichoderma viride*. *Mol. Microbiol*. **5**, 3007–3013.
8. Endo, Y., Glück, A. & Wool, I. (1991). Ribosomal RNA identity elements for ricin A-chain recognition and catalysis. *J. Mol. Biol*. **221**, 193–207.
9. Brigotti, M., Rambelli, F., Zamboni, M. & Montanaro, L. (1989). Effect of α-sarcin and ribosome-inactivating proteins on the interaction of elongation factors with ribosomes. *Biochem. J.* **257**, 723–727.
10. Moazed, D., Robertson, J.M. & Noller, H.F. (1988). Interaction of elongation factors EF-Tu with a conserved loop in 23S RNA. *Nature* **334**, 362–364.
11. Cundliffe, E., Cannon, M. & Davies, J. (1974). Mechanism of inhibition of eukaryotic protein synthesis by trichothecene fungal toxins. *Proc. Natl. Acad. Sci. USA* **71**, 30–34.
12. Lamy, B., Davies, J. & Schindler, D. (1992). The *Aspergillus* ribonucleolytic toxins (ribotoxins). In *Genetically Engineered Toxins.* (Frankel, A.E., ed), pp. 237–258, Marcel Dekker, Inc., NY.
13. Endo, Y. & Wool, I.G. (1982). The site of action of α-sarcin on eukaryotic ribosomes. *J. Biol. Chem*. **257**, 9054–9060.
14. Wool, I.G. (1984). The mechanism of action of the cytotoxic nuclease α-sarcin and its use to analyse ribosome structure. *Trends Biochem. Sci.* **9**, 14–17.
15. Endo, Y., Chan, Y.L., Lin, A., Tsurugi, K. & Wool, I.G. (1988). The cytotoxins α-sarcin and ricin retain their specificity when tested on a synthetic oligoribonucleotide (35-mer) that mimics a region of 28S ribosomal ribonucleic acid. *J. Biol. Chem*. **263**, 7917–7920.
16. Endo, Y., Glück, A., Chan, Y.L., Tsurugi, K. & Wool, I.G. (1990). RNA-protein interaction: an analysis with RNA oligonucleotides of the recognition by α-sarcin of a ribosomal domain for function. *J. Biol. Chem*. **265**, 2216–2222.
17. Glück, A. & Wool, I. (1996). Determination of the 28S ribosomal RNA identity element (G4319) for alpha-sarcin and the relationship of recognition to the selection of the catalytic site. *J. Mol. Biol*. **256**, 838–848.
18. Choe, S., *et al*., & Eisenberg, D. (1992). The crystal structure of diphtheria toxin. *Nature* **357**, 216–222.
19. Sixma, T., Pronk, S., Kalk, K., Zanten, B., Berghuls, A. & Hol, W. (1992). Lactose binding to heat-labile enterotoxin revealed by X-ray crystallography. *Nature* **355**, 561–564.
20. Olsnes, S. & Pihl, A. (1982). Toxic lectins and related proteins. In *Molecular Action of Toxins and Viruses.* (Cohen, P. & van Heyningen, S., eds), pp. 51–105, Elsevier Biomedical Press, Amsterdam.
21. Munoz, A., Castrillo, J.L. & Carrasco, L. (1985). Modification of membrane permeability during Semliki Forest virus infection. *Virology* **146**, 203–212.
22. Otero, M. J. & Carrasco, L. (1985). Proteins are cointernalized with virion particles during early infection. *Virology* **160**, 75–80.
23. Turnay, J., Olmo, N., Jimenez, A., Lizarbe, M. & Gavilanes, J. (1993). Kinetic study of the cytotoxic effect of α-sarcin, a ribosome inactivating protein from *Aspergillus giganteus*, on tumor cell lines: protein biosynthesis inhibition and cell binding. *Mol. Cell. Biochem.* **122**, 39–47.
24. Otero, M.J. & Carrasco, L. (1988). Exogenous phospholipase C permeabilizes mammalian cells to proteins. *Exp. Cell Res*. **177**, 154–161.
25. Gasset, M., Oñaderra, M., Thomas, P.G. & Gavilanes, J.G. (1990). Fusion of phospholipid vesicles produced by the anti-tumor protein α-sarcin. *Biochem. J.* **265**, 815–822.
26. Gasset, M., Oñaderra, M., Goormaghtigh, E. & Gavilanes, J.G. (1991). Acid phospholipid vesicles produce conformational changes on the antitumor protein α-sarcin. *Biochim. Biophys. Acta* **1080**, 51–58.
27. Oñaderra, M., Mancheno, J.M., Gasset, M., Lacadena, J. & Schiavo, G. (1993). Translocation of α-sarcin across the lipid bilayer of asolectin vesicles. *Biochem. J.* **295**, 221–225.
28. Brandhorst, T., Dowd, P.F. & Kenealy, W. (1996). The ribosome-inactivating protein restrictocin deters insect feeding in *Aspergillus restrictus*. *Microbiology* **142**, in press.
29. Lamy, L., Moutaouakil, M., Latge, J.P. & Davies, J. (1991). Secretion of a potential virulence factor, a fungal ribonucleotoxin, during human aspergillosis infections. *Mol. Microbiol*. **5**, 1811–1815.
30. Arruda, L.K., Mann, B.J. & Chapman, M.D. (1992). Selective expression of a major allergen and cytotoxin, *aspf I*, in *Aspergillus fumigatus*. *J. Immunol*. **149**, 3354–3359.
31. Brünger, A.T. (1993). *X-PLOR Manual Version 3.1: A System for X-ray Crystallography and NMR*. Yale University, New Haven, CT.
32. Hill, C., *et al.*, & Pavlovsky, S. (1983). The structural and sequence homology of a family of microbial ribonucleases. *Trends Biochem. Sci.* **8**, 364–369.
33. Heinemann, U. & Saenger, W. (1982). Specific protein-nucleic acid recognition in ribonuclease T1-2'-guanylic acid complex: an X-ray study. *Nature* **299**, 27–31.
34. Gohda, K., Oka, K., Tomita, K. & Hakoshima, T. (1994). Crystal structure of Rnase T1 complexed with the product nucleotide 3'GMP. *J. Biol. Chem*. **269**, 17531–17536.
35. Martinez-Oyanedel, J., Choe, H.W., Heinemann, U. & Saenger, W. (1991). Ribonuclease T1 with free recognition and catalytic site: crystal structure analysis at 1.5 Å resolution. *J. Mol. Biol*. **222**, 335–352.
36. Sevcik, J., Dodson, E. & Dodson, G. (1991). Determination and restrained least-squares refinement of the structures of ribonuclease Sa and its complex with 3'-guanylic acid at 1.8 Å resolution. *Acta Cryst*. B **47**, 240–253.
37. Mauguen, Y., *et al*., & Jack, A. (1982). Molecular structure of a new family of ribonucleases. *Nature* **297**, 162–164.
38. Zegers, I., Verhelst, P., Choe, H.W., Heinemann, U., Saenger, W. & Wyns, L. (1992). Role of Histidine-40 in ribonuclease T1 catalysis: three-dimensional structures of the partially active His40Lys mutant. *Biochemistry* **31**, 11317–11325.
39. Noguchi, S., Satow, Y., Uchida, T., Sasaki, C. & Matsuzaki, T. (1995). Crystal structure of Ustilago sphaerogena ribonuclease U2 at 1.8 Å resolution. *Biochemistry* **3**, 15583–15591.
40. Yang, R. & Kenealy, W. (1992). Effects of amino-terminal extensions and specific mutations on the activity of restrictocin. *J. Biol. Chem*. **267**, 16801–16805.
41. Nishikawa, S., *et al*., & Ikehara, M. (1987). Two histidines are essential for ribonuclease T1 activity as is the case for ribonuclease A. *Biochemistry* **26**, 8620–8624.
42. Campbell, R. & Petsko, G. (1987). Ribonuclease structure and catalysis: crystal structure of sulfate-free native ribonuclease A at 1.5 Å resolution. *Biochemistry* **26**, 8579–8584.
43. Steyaert, J., Hallenga, K., Wyns, L. & Stanssens, P. (1990). Histidine-40 of ribonuclease T1 acts as base catalyst when the true catalytic base, glutamic acid-58, is replaced by alanine. *Biochemistry* **29**, 9064–9072.
44. Ding, J., Koellner, G., Grunert, H.P. & Saenger, W. (1991). Crystal structure of ribonuclease T1 complexed with adenosine 2'-monophosphate at 1.8 Å resolution. *J. Biol. Chem.* **266**, 15128–15134.
45. Kostrewa, D., Choe, H.W., Heinemann, U. & Saenger, W. (1989). Crystal structure of guanosine-free ribonuclease T1 complexed with vanadate (V) suggests conformational change upon substrate binding. *Biochemistry* **28**, 7592–7600.
46. Szewczak, A., Moore, P., Chan, Y.L. & Wool, I.G. (1993). The conformation of the sarcin/ricin loop from 28S ribosomal RNA, *Proc. Natl. Acad. Sci. USA* **90**, 9581–9585.
47. Montfort, W., *et al.*, & Robertus, J. (1987). The three-dimensional structure of ricin at 2.8 Å. *J. Biol. Chem*. **262**, 5398–5403.
48. Rutenber, E., Ready, M. & Robertus, J. (1987). Structure and evolution of ricin B chain. *Nature* **326**, 624–626.
49. Rutenber, E. & Robertus, J. (1991). Structure of ricin B-chain at 2.5 Å resolution. *Proteins- Struct. Funct. and Genet.* **10**, 260–269.
50. Weis, W., Kahn, R., Fourme, R., Drickamer, K. & Hendrickson, W. (1991). Structure of the calcium-dependent lectin domain from a rat mannose-binding protein determined by MAD phasing. *Science* **254**, 1608–1615.
51. Rini, J., Hardman, K., Einspahr, H., Suddath, F. & Carver, J. (1993). X-ray crystal structure of a pea lectin-trimannoside complex at 2.6 Å resolution. *J. Biol. Chem*. **268**, 10126–10132.
52. Banerjee, R., *et al*., & Vijayan, M. (1994). Crystal structure of peanut lectin, a protein with an unusual quaternary structure. *Proc. Natl. Acad. Sci. USA* **91**, 227–231.
53. Weis, W. (1994). Lectins on a roll: the structure of E-selectin. *Structure* **2**, 147–150.
54. Bajorath, J. & Aruffo, A. (1994). Molecular model of the extracellular lectin-like domain in CD69. *J. Biol. Chem*. **269**, 32457–32463.
55. Hollenbaugh, D., Bajorath, J., Stenkamp, R. & Aruffo, A. (1993). Interactions of P-selectin (CD62) and its cellular ligand: analysis of critical residues. *Biochemistry* **32**, 2960–2966.
56. Martinez, S. & Smith, J. (1991). Crystallization and preliminary characterization of mitogillin, a ribosomal ribonuclease from *Aspergillus restrictus*. *J. Mol. Biol*. **218**, 489–492.

57. Getzoff, E.D., *et al*., & Westbrook, E.M. (1993). Laue diffraction protein crystallography at the National Synchrotron Light Source. *Nucl. Instrum. Meth. Phys. Res*. B 79, 249–55.
58. Ren, Z. & Moffat, K. (1995). Quantitative analysis of synchrotron Laue diffraction patterns in macromolecular crystallography. *J. Appl. Cryst*. 28, 461–481.
59. Ren, Z. & Moffat, K. (1995). Deconvolution of energy overlaps in Laue diffraction, *J. Appl. Cryst*. 28, 482–493.
60. Ren, Z. & Moffat, K. (1994). Laue crystallography for studying rapid reactions. *J. Synchrotron Rad*. 1, 78–82.
61. McRee, D.E. (1992). A visual protein crystallographic software system for X11/XView. *J. Mol. Graph*. 10, 44–46.
62. Collaborative Computational Project, Number 4. (1994). The CCP4 suite: programs for protein crystallography. *Acta Cryst*. D 50, 760–763.
63. Laskowski, R.A., MacArthur, M.W., Moss, D.S. & Thornton, J.M. (1993). PROCHECK: a program to check the stereochemistry of protein structures. *J. Appl. Cryst*. 26, 283–291.
64. Jones, T.A., Zhou, J.Y., Cowan, S.W. & Kjeldgaard, M. (1991). Improved methods for building protein models in electron density maps and the location of errors in these models. *Acta Cryst*. A 47, 110–119.
65. Nicholls, A., Sharp, K.A. & Honig, B. (1991). Protein folding and association: insights from the interfacial and thermodynamic properties of hydrocarbons, *Proteins- Struct. Funct. Genet*. 11, 281–296.
66. Kraulis, P.J. (1991). MOLSCRIPT: a program to produce both detailed and schematic plots of protein structures. *J. Appl. Cryst*. 24, 946–950.
67. Evans, S.V. (1993). SETOR: hardware lighted three-dimensional solid model representation of macromolecules. *J. Mol. Graph*. 11, 134–138.